Analysis of high contrast grating biosensor using surface plasmon resonance for enhanced sensitivity and detection accuracy

PALLAVI SHARMA[1], PRADEEP KUMAR TEOTIA[2], R. S. KALER[1,*]
[1]*ECE Department, Thapar Institute of Engineering and Technology, Patiala, 147004, India*
[2]*Delhi Technological University, Bawana Road, Delhi, 110042, India*

A high contrast grating-based surface Plasmon resonance-based biosensor with high detection accuracy has been proposed. High sensitivity has been obtained by using a high value of dielectric material. The detection accuracy and sensitivity are optimized utilizing the metal layer thickness and its width in the continuation of periodic gratings. With the help of the finite difference time domain (FDTD), the enhanced values are obtained and compared to the photonic crystal waveguide and surface plasmon resonance sensor. The proposed sensor also overlaps the fabrication constraints of various metals as a high value of dielectric material has been employed.

(Received August 2, 2024; accepted February 3, 2025)

Keywords: High Contrast Gratings, Surface Plasmon, Bio-Sensors, Thin films

1. Introduction

The phenomena occurring in surface plasmon resonance (SPR) waveguides improve the pattern of biosensors in terms of sensitivity, robustness, and compactness. The theory behind the SPR waveguide concept includes the electromagnetic wave theory. In all photonic integrated circuits, the propagation of light or electromagnetic waves is a significant aspect. To achieve good selectivity and sensitivity, the selection of material (i.e., dielectric or metal) having good optical properties (reflectance and transmittance) has gained attention from the research fraternity [1]. Many groups of researchers have explored the optical properties of many metamaterials. Further, miniaturization of dimensions or structures of photonic devices has also been achieved in patterning [2]. During the past few years, the discovery of near-wavelength grating structures has proliferated. The medium of high index is constrained by low-index materials mentioned as an HCS i.e. high contrast subwavelength grating. Further, technology advancement in lithography researchers contributed actively in the field of High Contrast Grating.

In 2017, we proposed a novel grating multilayer-based biosensor prototype to detect lung cancer using the Vroman effect [3]. Zhuo Li et al. [4] demonstrated the HCG-based SPPW (spoof surface plasmon resonance waveguide) which further opened a window for ultra-low loss SPP waveguides. They also elaborated that HCG-based SPPs are much better than metal grating-based SPPs subject to the geometry and medium parameters engineering. In continuation of that, HCG also shows properties to be a prominent biosensor [5]. Fang et al. [6] demonstrated a polarization-independent filter using an HCSG structure to achieve high reflectivity using grating width, thickness, periods, and angle of incidence. As grating parameters increase and the angle of incidence decreases, the reflectivity of the HCSG structure increases. The bimetallic layered structure using high contrast grating has a good penetration depth of surface plasmon modes in the dielectric region [7]. Better computational techniques made it easier to understand the behavior of plasmonic modes in HCG. Similarly, it has been easier to fabricate metallic HCG for biosensing applications [8]. It is represented in the study presented in [14] that high-quality factors can be achieved by optimizing the grating period, duty cycle, and thickness of the substrate. Another study [15] shows that Silica-based photonic crystal slabs when utilized with graphene show superior sensing performance and can be promoted for refractive index-based sensing applications.

HCG-based sensing is helpful in many areas like HCG can be utilized to create the kinetic and thermodynamic data on antibodies that are surface-attached with the respective antigens [22]. Other study shows pedestal HCG [23-24] can show bulk and surface sensitivity more than the basic HCG structures. GaN-HCG-based sensor structures can help in applications areas like IoT for refractive index sensing [25].

Previously, only metals have shown good dispersion characteristics as well as plasmonic behavior of Gold (Au), Silver (Ag) & Aluminium (Al) etc. [31] But, West et al. [9] paved a new way for alternate plasmonic materials, which showed the same characteristics as plasmonic metals. Some other researchers utilized codings [26-28] and signal analysis [29, 32-34] for the improvement of sensitivity [30]. Similarly, Teotia et al. [3] proposed a multi-layered bimetallic structure using a high dielectric region. Painam [10] also presented a prototype of the biochemical sensor to detect chemical concentration using a photonic crystal waveguide.

The above biosensors use different technologies of Surface plasmon resonance and a photonic crystal waveguide but have specific sensitivity and detection accuracy limitations. To meet the best configuration, we have investigated HCG-based plasmonic biosensors using Indium Tin Oxide (ITO) and Gold (Au).

2. Proposed setup

The proposed HCG-based plasmonic biosensor is shown in Fig. 1. It includes a layered structure having a metal surrounded by high-contrast dielectric material with efficiently managed gratings. The proposed structure of the waveguide is made up of a dielectric silica layer with a refractive index of 1.44 and another stacked dielectric silicon layer with a refractive index of 3.42. For better sensitivity and detection capability, air holes must be added in structuring HCG-based biosensors. This is also done to improve the all-over performance of the sensor. The air hole inclusion will help in increasing the interaction between the biomolecules and guided light. This will further improve the biomolecular binding and hence, the sensitivity of the sensor.

If there are no air holes, mode resonance effects will be weakened, and sharp dips will be observed. HCG air holes produce a high contrast refractive index between material and medium. If these air holes are removed, it will decrease the contrast and can create weak confinement. This will lower the overall reflectivity. Furthermore, the absence of airholes can weaken the Bragg reflection which will further reduce the efficient reflection ability of structure for certain wavelengths. Hence inclusion of air holes has a significant role.

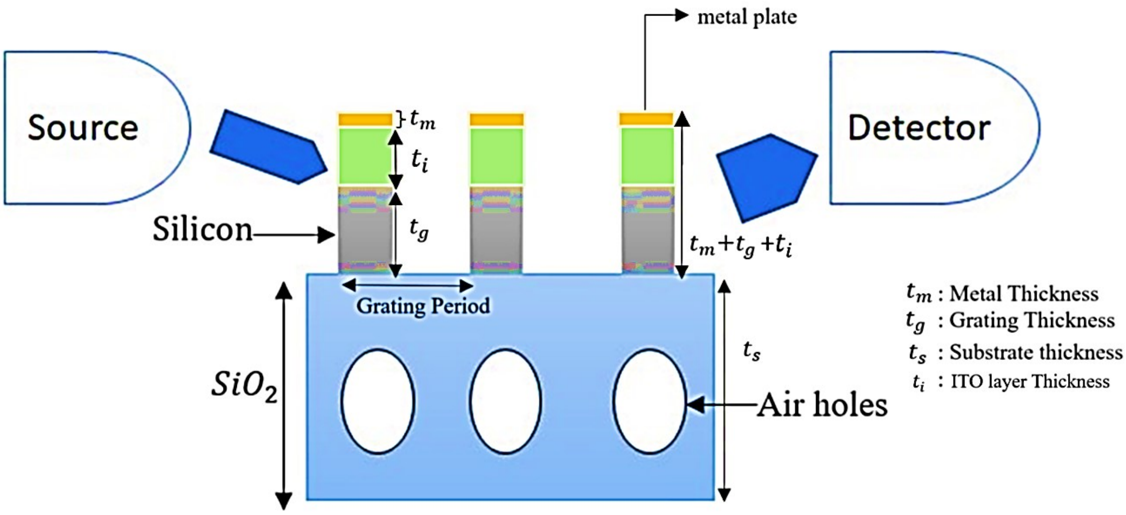

Fig. 1. Geometry of proposed HCG-based biosensor (colour online)

2.1. Analysis of HCG using plasmon resonance

The proposed structure is covered by a periodic grating of 50 nm which is filled with air (η=1.0). Further, the metal layer at the top is monitored by the analyte. The proposed geometry consists of an interface of metal and dielectric, which is modulated by periodic gratings. According to the Bloch-Floquet condition shown in equation (1) [11]:

$$k_{xn} = k_x + n.\frac{2\pi}{d} \tag{1}$$

Floquet theorem states that a TM (Transverse Magnetic) polarised wave strikes the structure's surface as defined in Fig. 1 with free space number i.e., $k_0(k_0 = \frac{\omega}{c_0}$, ω = wave number and c_o = velocity of light) will produce strong Bloch waves. Usually, in the SPP conditions of the sensing area, it is said that resonance wavelength is truly sensitive to refractive index variations of the analyte of the sensor (using the wavelength interrogation method) [11]. A defined ray from a light source is made to pass through the above-said waveguide using appropriate photonic devices. An optical photodetector can detect the same light for further observations. By wavelength interrogation, a wavelength (transmission) spectrum shows a minimum value at resonance wavelength. A small change in the analyte's refractive index causes a good shift in the wavelength spectrum called refractive index sensing.

Generally, the biosensor may be evaluated in terms of detection accuracy and sensitivity. Sensitivity 'Sn' can be expressed by following equation (2) for 'λ': wavelength and 'RI' as refractive index [11]:

$$S_n = \frac{\delta\lambda}{\delta\,(RI)} \tag{2}$$

While detection accuracy can be expressed w.r.t. full width at half maximum (FEHM) by the following equation (3) [11]:

$$DA = \frac{1}{FWHM} \quad (3)$$

To approach a better design of biosensors in the case of SPP with HCG, the thickness of the metal and dielectric layer has to be determined in such a manner that the TM wave can be excited. For more understanding of p-polarised wave at the output of waveguide, an equation with respect to Flouqet theorem and Bloch waves can be expressed by equation (4) [12]. In equation 4, for studying the p-polarized light, the transmitted power P(f) is studied in terms of normalized power to source hence, it is also called normalized transmitted power as a function of frequency.

$$P(f) = e^{-4\pi\, img(n_{eff})\frac{L}{\lambda}} \quad (4)$$

where $\eta_{eff} = the$ effective refractive index of design. In surface plasmon resonance, the imaginary part of metal can be better responsible for a better dip in the resonance wavelength. A sequence of iterations or simulations has been done to investigate and optimize the performance of the proposed biosensor using the Finite Division Time Domain Method.

3. Results and discussion

To carry out the simulations, the substrate's refractive index has been assumed as n_s = 1.0. For a better understanding of the impact of the metal layer with high contrast grating, the following variations have been observed (i) gratings with ITO and (ii) gratings with Au-ITO, including the parameters mentioned above. The dielectric constants for Gold (Au), ITO, Silica, and Silicon (Si) are referred from Palik et al. [13].

The Magnetic field H_y has been observed about the variation of metal layers as shown in Fig. 2. Fig. 2 shows that as the metal layer increases, the depth of surface plasmon waves has also increased. As already mentioned earlier, the High contrast grating provides strong SPP waves at the metal and dielectric interface.

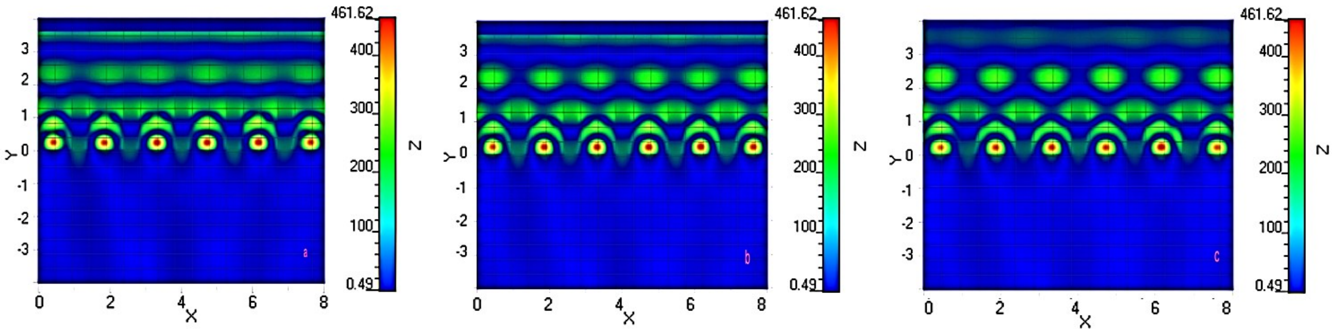

(a) (b) (c)

Fig. 2. Variation of surface plasmons at a different thickness (a) 40 nm (b) 50 nm (c) 60 nm (colour online)

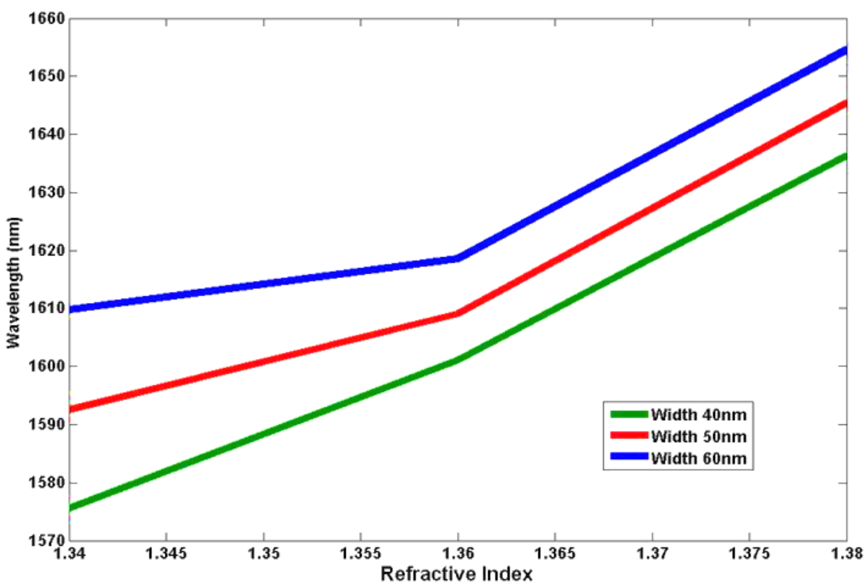

Fig. 3. Graphical variation in resonance wavelength with metal thickness w.r.t. refractive index (colour online)

Further, the transmittance was also calculated by taking specific parameters constant, as shown in Fig. 3. It has been assumed that the interaction length is almost equal to the coupling wavelength. The power has been kept virtually equal to unity.

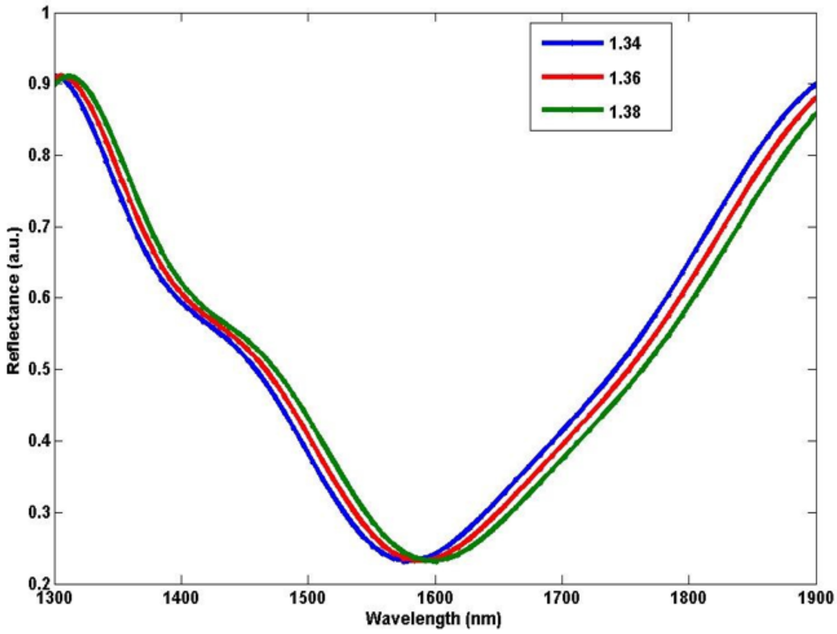

Fig. 4. Reflectance of HCG-based biosensor at η = 1.34, 1.35, and 1.36 (colour online)

Our previous work [2-3] has figured out that many metals have sharp transmission curves, but they also have constraints in fabrication. The use of HCG makes it easier for researchers to fabricate the design much more accessible. For no metal presence, two possibilities of field distribution are there: First, extension of field to analyte makes an evanescent wave which is essential for bio-sensor applications. This will further interact with the molecules and also help in the detection of any refractive index changes. Second, the field confined by the high-refractive index regions of the grating itself will create the field distribution.

The reflection response of HCG with no metal layer can depend on various factors like grating thickness, refractive index, and wavelength of the incident light. The geometry like the thickness of HCG can help in determining the resonant wavelengths where usually high reflectivity is observed. It further affects the sharpness and strength of the reflection response. We have also shown the changes w.r.t. refractive index where the dip is observed at 1600 nm. These sharp and narrow dips at 1600 nm show that the light is properly coupled to guided modes of the grating and further indicate that it is not reflected. These types of observations help in making HCG suitable as a refractive index-based sensor.

Generally smaller value of $\delta\lambda$ reflects the weaker interaction of surface plasmon at metal - analyte interface. The reflection response of HCG with no metal layer can depend on various factors like grating thickness, refractive index, and wavelength of the incident light. The geometry like the thickness of HCG can help in determining the resonant wavelengths where usually high reflectivity is observed. It further affects the sharpness and strength of the reflection response.

We have also shown the changes w.r.t. refractive index where the dip is observed at 1600 nm. These sharp and narrow dips at 1600 nm show that the light is properly coupled to guided modes of the grating and further indicate that it is not reflected. These types of observations help in making HCG suitable as a refractive index-based sensor.

It is observed that the stronger interactions between the analyte and the field is occurring at longer wavelengths. The reason for this is penetration of evanescent field is extended further at longer wavelengths that also helps the structure to detect the minor changes in the refractive index. Hence, higher sensitivity will be achieved.

But Fig. 4 shows the overall value of $\delta\lambda$, which indicates the strong interaction of surface plasmons. The presence of gratings in high-contrast grating sensors not only improves the sensor characteristics but also impacts the sensitivity and stability. The insertion of the gold layer above the ITO layer enhances the sensor's performance in terms of accuracy. It is also worth mentioning that the transmittance also got reduced due to the high value of the dielectric constant, which alters the interaction of surface plasmon resonance. Still, it will not affect the sensitivity and detection accuracy.

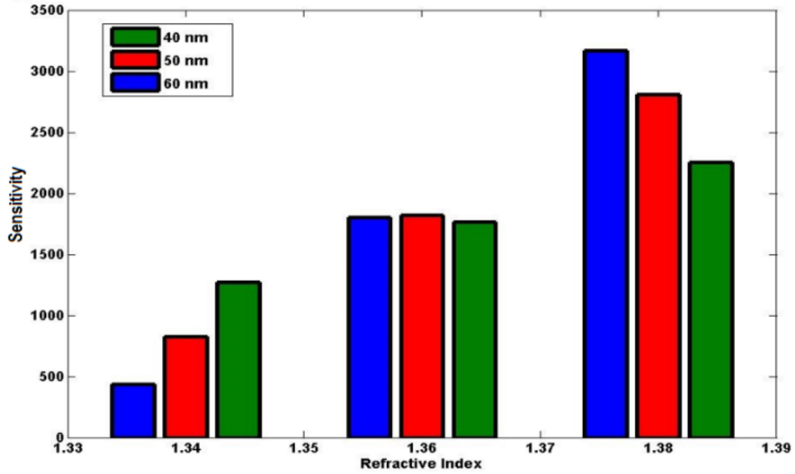

Fig. 5. Sensitivity variation w.r.t refractive index at a different metal thickness (colour online)

For more understanding of modal fields as shown in Fig. 2, the SPP waves have strong interaction over analyte to metal. This also shows more penetration depth than the Photonic Crystal Waveguide and Surface plasmon resonance as mentioned in [2-3]. In terms of performance, detection accuracy and sensitivity for the high contrast grating sensor have been calculated. The sensitivity is shown in Fig. 5, while the detection accuracy is shown in Fig. 6. The following equation 5 shows the formula for the measurement of the sensitivity of an HCG-biosensor. It is the ratio resonance wavelength shift to the unit change that occurred in the refractive index of the medium.

$$S_\lambda = \frac{\lambda_{resonance}}{\Delta\lambda} \tag{5}$$

Fig. 5 indicates that the sensitivity of the sensor increases with the thickness of the metal layer. The sensitivity at a refractive index of 1.36 was reported as 3150 nm-RIU^{-1}.

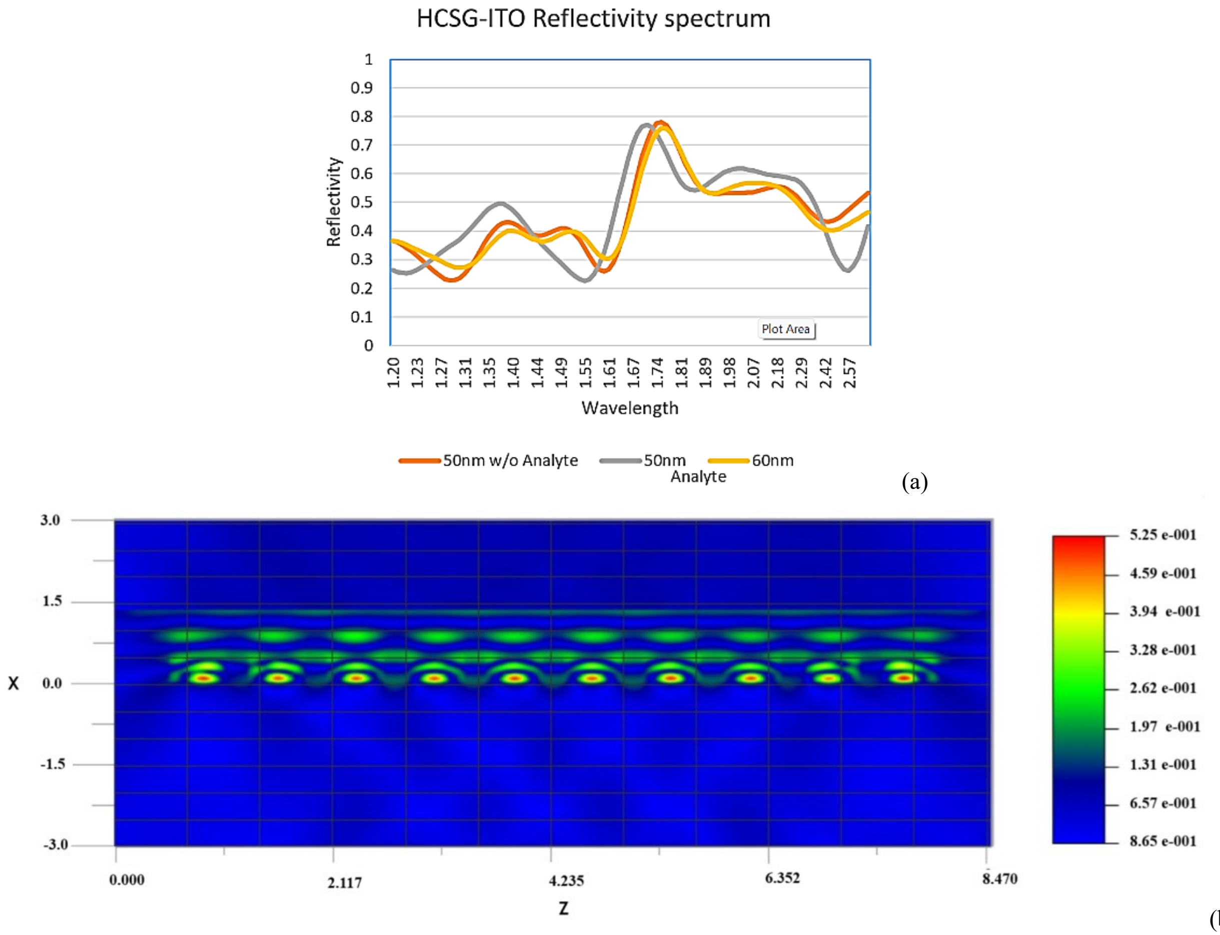

Fig. 6. Illustration of resonance shift with the insertion of analyte and without analyte (a) Graphical (b) EH distribution with analyte layer (colour online)

The graph in the above Fig. 6 represents the reflectivity plot for HCSG with ITO Layer with different widths 50 nm, 60 nm, and 50 nm with analyte. From the obtained result, it has been observed that there is a wavelength shift by changing the width of the ITO layer. Another shift is observed by inserting the analyte as the top thin layer. The shift that occurred is proportional to the variation that occurred in the refractive indices which is triggered by the presence of the analyte. This happens when the analyte is bound to the surface of the sensor, it causes variation in the local refractive index. HCG-based sensors have been highly sensitive to these variations. This further causes changes in the effective refractive index of the mode, hence resulting in a resonance shift.

Table 1 shows the comparison of the sensitivity of the various types of SPR sensors reported in the previous literature with the proposed structure's sensitivity. It also shows the simulated structure is more superior in comparison to others.

Table 1. Sensitivity comparison of the proposed system with previously reported techniques

Ref. No.	Sensor Utilized	Technique/Characteristics	Sensitivity (nm-RIU^{-1})
[16]	Internal-coated SPR	Conducting metal oxide film for IR region	1310
[17]	Internal-coated SPR	Tapered optical fibers for the visible region	2000
[18]	Internal-coated SPR	Double resonance dips	1929
[19]	Internal-coated SPR	Birefringent microstructured optical fiber	3100
[20]	External-coated SPR	D-shaped fiber with a solid core	2000
[21]	External-coated SPR	Multi-hole fiber	2000
Proposed Work			**3150**

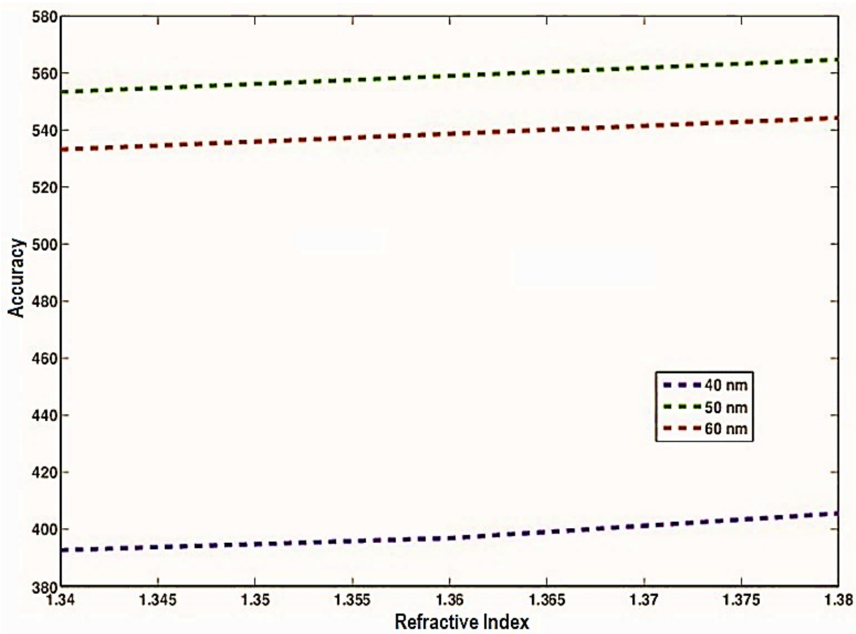

Fig. 7. Detection accuracy variation graph w.r.t refractive index at different metal thickness (colour online)

From Fig. 7, transmittance can be described better with w.r.t sensitivity and detection accuracy at a metal thickness layer 50 nm. The detection accuracy was 560 μm^{-1} at a refractive index beyond 1.37. In comparison to the [3], a good increment in detection accuracy has been observed, while sensitivity has been slightly reduced which in turn proved a good biosensor in comparison [3].

4. Conclusion

We have reported and investigated High contrast grating SPP biosensors that overlap the fabrication constraints by using a high value of dielectric materials. In comparison to the Photonic crystal waveguide and surface plasmon resonance sensor, the reported sensor exhibits a higher resolution in terms of detection accuracy. The presence of high contrast grating provides stability and improves the detection accuracy 560 μm^{-1} and sensitivity 3150 nm-RIU^{-1}. The value of a high dielectric constant enhances the interaction of surface plasmon resonance and also has the lowest influence on sensitivity DA and S_n. A high value of dielectric constant and periodic grating provides a possibility for this geometry to be acknowledged in any wavelength spectral domain.

Declarations

Competing interests
The authors declare that they have no known conflicts of interest associated with this publication.

Author's Contribution
All authors contributed to the study's conception and design. All authors read and approved the final manuscript.

Funding
The authors declare that no funds, grants, or other support were received during the preparation of this manuscript

Data Availability
Data sharing is not applicable to this article as no datasets were generated or analysed during the current study.

References

[1] M. J. Heck, J. F. Bauters, M. L. Davenport, D. T. Spencer, J. E. Bowers, Laser & Photonics Reviews **8**, 5 (2014).
[2] P. K. Teotia, R. Kaler, Optics Communications **395**, 154 (2017).
[3] P. K. Teotia, R. Kaler, Optics Communications **406**, 188 (2018).
[4] Z. Li, B. Xu, L. Liu, J. Xu, C. Chen, C. Gu, Y. Zhou, Scientific Reports **6**, 1 (2016).
[5] D. Urbonas, R. F. Mahrt, T. Stoferle, Light: Science & Applications **10**, 1 (2021).
[6] W. Fang, C. Yue, X. Fan, H. Niu, X. Zhang, H. Xu, N. K. Chen, C. Bai, Asia Communications and Photonics Conference, Optical Society of America, pp. Su2A–129 (2018).
[7] Y. Zhou, V. Karagodsky, B. Pesala, F. G. Sedgwick, C. J. Chang-Hasnain, Optics Express **17**, 3 (2009).
[8] V. Myroshnychenko, J. Rodrıguez-Fernandez, I. Pastoriza-Santos, A. M. Funston, C. Novo, P. Mulvaney, L. M. Liz-Marzan, F. J. G. de Abajo, Chemical Society Reviews **37**, 9 (2008).
[9] P. R. West, S. Ishii, G. V. Naik, N. K. Emani, V. M. Shalaev, A. Boltasseva, Laser & Photonics Reviews **4**, 6 (2010).
[10] B. Painam, R. Kaler, M. Kumar, Plasmonics **12**, 899 (2016).
[11] A. K. Sharma, B. Gupta, Optics Communications **245**, 1 (2005).
[12] Y. Al-Qazwini, P. Arasu, A. Noor, Photonics (ICP), 2011 IEEE 2nd International Conference on, IEEE, pp. 1–4 (2011).
[13] E. D. Palik, Handbook of Optical Constants of Solids, Vol. **3** (Academic Press, 1998).
[14] Yi-Wen Lin, Tsun-Hsu Chang, Tsing-Hua Her, Hsin-Yu Yao, Optics Express **32**(20), 36048 (2024).
[15] T. Sang, S. A. Dereshgi, W. Hadibrata, I. Tanriover, K. Aydin, Nanomaterials **11**(2), 484 (2021).
[16] R. K. Verma, B. D. Gupta, J. Opt. Soc. Am. A **27**, 846 (2010).
[17] M.-C. Navarrete, N. Díaz-Herrera, A. González-Cano, Ó. Esteban, Sens. Actuators B **190**, 881 (2014).
[18] N. K. Sharma, M. Rani, V. Sajal, Sens. Actuators B **188**, 326 (2013).
[19] N. M. Y. Zhang, D. J. J. Hu, P. P. Shum, Z. Wu, K. Li, T. Huang, Lei Wei, J. Opt. **18**, 065005 (2016).
[20] J. N. Dash, R. Jha, IEEE Photonics Technol. Lett. **26**, 595 (2014).
[21] D. Gao, C. Guan, Y. Wen, X. Zhong, L. Yuan, Opt. Commun. **313**, 94 (2014).
[22] T. Sun, S. Kan, G. Marriott, C. Chang-Hasnain, Sci. Rep. **6**, 27482 (2016).
[23] L. Y. Beliaev, Peter Groth Stounbjerg, Giovanni Finco, A.-I. Bunea, R. Malureanu, L. René Lindvold, Osamu Takayama, Peter E. Andersen, Andrei V. Lavrinenko, Nanomaterials **12**, 1748 (2022).
[24] L. Y. Beliaev, S. Kim, B. F. S. Nielsen, M. V. Evensen, Ada-Ioana Bunea, Radu Malureanu, Lars Lindvold, Osamu Takayama, Peter E. Andersen, Andrei V. Lavrinenko, ACS Appl. Nano Mater. **6**(13), 12364 (2023).
[25] Y. Takashima, M. Haraguchi, Y. Naoi, Sensors **20**, 4444 (2020).
[26] S. Singh, R. S. Kaler, Optik **124**(15), 2131 (2013).
[27] K. S. Bhatia, R. S. Kaler, T. S. Kamal, R. Randhawa, Optik **124**(2), 117 (2013).
[28] V. Jyoti, R. S. Kaler, Optik **122**, 10 (2011).
[29] R. S. Kaler, T. S. Kamal, A. K. Sharma, S. K. Arya, R. A. Agarwala, Fiber and Integrated Optics **21,** 3 (2002).
[30] M. Verma, R. S. Kaler, Optik **244**, (2021).
[31] R. S. Kaler, T. S. Kamal, A. K. Sharma, Fiber Integrated Optics **21**, 5 (2002).
[32] A. K. Garg, R. S. Kaler, Chinese Optics Letters **6**, 4 (2008).
[33] H. Kaur, R. S. Kaler, Journal of Nonlinear Optical Physics & Materials **32**, 3 (2023)
[34] A. K. Garg, R. S. Kaler, Chinese Optics Letters **6**, 11 (2008).

*Corresponding author: drrajindersinghkaler@gmail.com